Supplement of Hydrol. Earth Syst. Sci., 29, 903–924, 2025
https://doi.org/10.5194/hess-29-903-2025-supplement

Hydrology and Earth System Sciences
Open Access
EGU

Supplement of

Exploring the potential processes controlling changes in precipitation–runoff relationships in non-stationary environments

Tian Lan et al.

Correspondence to: Tongfang Li (tongfangli@chd.edu.cn) and Hongbo Zhang (hbzhang@chd.edu.cn)

Contents of this file

Introduction

This supporting information includes the information on hydrological monitoring stations and meteorological stations selected in this study. The calculation of daily potential evapotranspiration and baseflow, the implementation of TFPW-MK, TFPW-BS-Pettitt, and Maximal Information Coefficient are also introduced in detail here.

S1 Information of data in the study area

Table S1. The information on hydrological monitoring stations selected in this study.

Stations	Drainage area (km^2)	Duration	Longitude (°E)	Latitude (°N)
Qinan	9712	1965-2014	105.07	35.68
Weijiabao	36335	1960-2014	105.02	35.38
Xianyang	44840	1960-2014	105.65	36.57
Zhangjiashan	43161	1960-2019	106.27	36.00
Zhuangtou	25173	1960-2007	105.72	35.97

Table S2. The information on meteorological stations selected in this study.

No.	Stations	Longitude (°E)	Latitude (°N)	No.	Stations	Longitude (°E)	Latitude (°N)
1	**Lintao**	103.87	35.37	20	**Huating**	106.62	35.20
2	**Huining**	105.07	35.68	21	**Changwu**	107.80	35.20
3	**Huajialing**	105.02	35.38	22	**Huachi**	107.98	36.45
4	**Yanchi**	107.38	37.80	23	**Zhengning**	108.40	35.48
5	**Dingbian**	107.58	37.58	24	**Ningxian**	107.92	35.52
6	**Wuqi**	108.17	36.92	25	**Luochuan**	109.42	35.77
7	**Haiyuan**	105.65	36.57	26	**Tongchuan**	109.07	35.08
8	**Guyuan**	106.27	36.00	27	**Minxian**	104.02	34.43
9	**Huanxian**	107.30	36.57	28	**Tianshui**	105.75	34.58
10	**Qingcheng**	107.90	35.98	29	**Zhenan**	109.15	33.43
11	**Zhidan**	108.77	36.77	30	**Baoji**	107.13	34.35
12	**Yanan**	109.45	36.58	31	**Fengxiang**	107.38	34.52
13	**Ganquan**	109.35	36.27	32	**Wugong**	108.23	34.32
14	**Xiji**	105.72	35.97	33	**Xian**	108.93	34.30
15	**Kongtong**	106.67	35.55	34	**Yaoxian**	108.98	34.93
16	**Zhuanglang**	106.07	35.22	35	**Huashan**	110.08	34.48
17	**Xifengzhen**	107.63	35.73	36	**Jinghe**	108.97	34.43
18	**Zhenyuan**	107.18	35.68	37	**Foping**	107.98	33.52
19	**Jingchuan**	107.35	35.35	38	**Shangzhou**	109.97	33.87

S2 Calculating daily potential evapotranspiration and baseflow

The daily baseflow is estimated using the Chapman-Maxwell filter method (*Eq*. (S1)), which assumes a linear relationship between baseflow and antecedent groundwater recharge, while surface runoff is assumed to be a nonlinear function of rainfall intensity (Chapman, 1999).

$$Q_{\mathrm{b}}(i) = \frac{k}{2-k} Q_{\mathrm{b}}(i-1) + \frac{1-k}{2-k} Q(i) \tag{S1}$$

where $Q_{\mathrm{b}}(i)$ and $Q(i)$ are baseflow and total runoff (mm) at time interval i, respectively, and the parameter k is the recession constant during periods of no direct runoff, which is set to 0.95(Hu et al., 2021).

The calculation of daily ET_0 for the sub-basins, which represents the reference evapotranspiration, was carried out using the FAO Penman-Monteith equation (*Eq*. (S2)), a well-established and widely used method (Cai et al., 2007).

$$ET_0 = \frac{0.408\Delta(R_\mathrm{n} - G) + \gamma \frac{900}{T + 273} u_2 (e_\mathrm{s} - e_\mathrm{a})}{\Delta + \gamma(1 + 0.34u_2)} \quad \text{(S2)}$$

where ET_0 is the reference evapotranspiration (mm day^{-1}); R_n is the net radiation (MJ m^{-2} day^{-1}); G is the soil heat flux density (MJ m^{-2} day^{-1}); T is the mean daily air temperature (°C); u_2 is the wind speed at 2 m height (m s^{-1}); e_s is the saturation vapour pressure (kPa); e_a is the actual vapour pressure (kPa); Δ is the slope vapour pressure curve (kPa °C^{-1}); γ is the psychrometric constant (kPa °C^{-1}).

S3 Methodology flow of this study

The non-stationary hydrological processes in the study area were initially identified using Trend-Free Pre-Whitening and Binary Segmentation techniques (TFPW-BS-Pettitt) and Mann-Kendall (TFPW-MK). To comprehend the potential driving mechanisms affecting the PRR within non-stationary hydrological processes, we introduce a novel index termed the (Dynamic) Driving index for changes in Precipitation-Runoff Relationships (DPRR or D-DPRR). Investigating the candidate driving factors for changes in PRR in non-stationary processes, we consider climate forcing, groundwater, vegetation dynamics, and anthropogenic influences. The nonlinear correlations among the factors were assessed. Based on the candidate driving factors, we develop a comprehensive conceptual model of catchment response, integrating plausible explanations that align with empirical evidence and logical reasoning. By incorporating the driving levels and directions of each driving factor computed from DPRR and D-DPRR into the conceptual model, the possible process explanations for changes in the PRR in the study area were deduced. It is crucial to emphasize that changes in precipitation-runoff relationships involve two aspects: variations in PRR before and after the influence of driving factors and changes in PRR in non-stationary conditions. The flowchart is illustrated in Figure S1, and its codes are opened (if you have interest in codes, please do not hesitate to contact us).

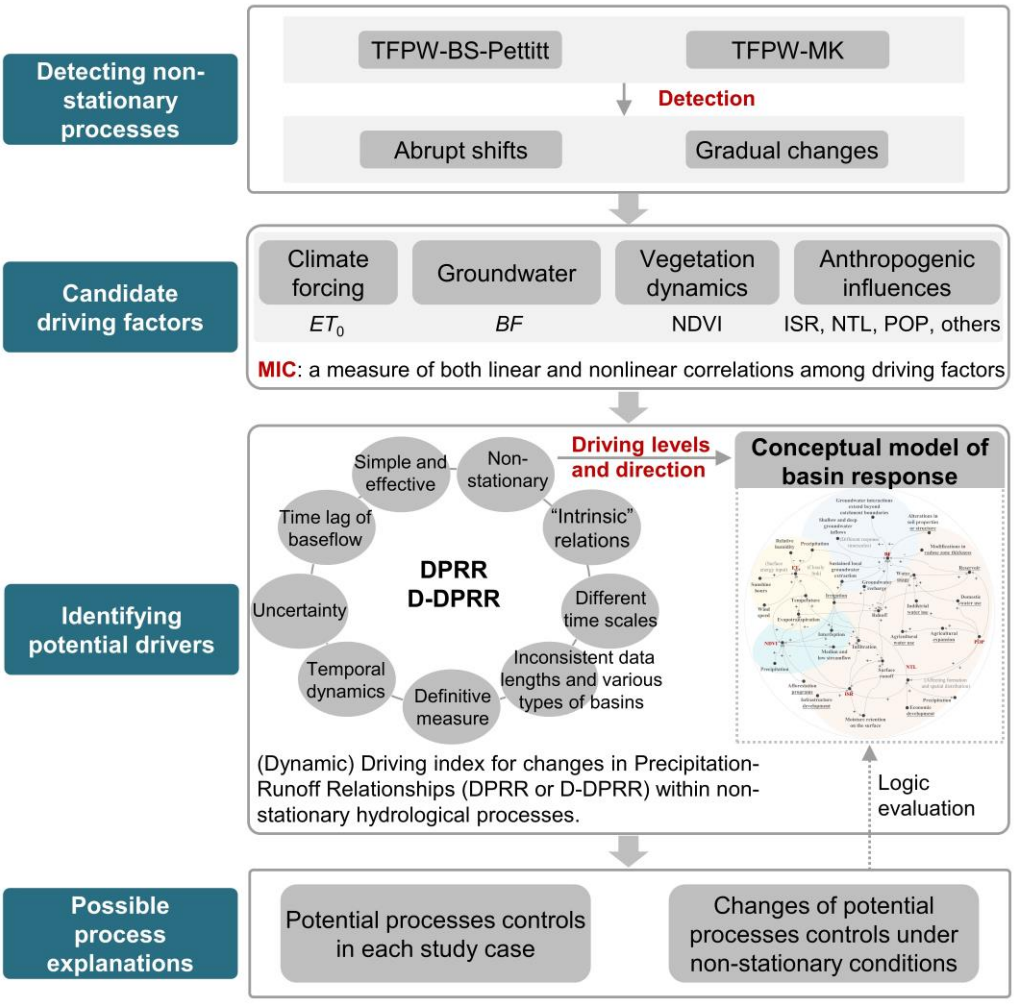

Figure S1. Integrated framework for exploring the potential processes controlling changes in precipitation-runoff relationships in non-stationary environments.

S4 Techniques for abrupt and gradual changes of temporal series related to catchments

S4.1 Trend-free pre-whitening Mann-Kendall test (TFPW-MK)

The non-parametric Mann-Kendall (MK) statistical test is a widely accepted method recommended by the World Meteorological Organization (WMO) for assessing trends or gradual changes in meteorological and hydrological time series (Douglas et al., 2000; Hamed and Rao, 1998; Kendall, 1975; Mann, 1945; Yue et al., 2002b; Yue and Wang, 2004). The Mann-Kendall test statistic can be stated as follows:

$$S = \sum_{k=1}^{n-1}\sum_{j=k+1}^{n}\mathrm{sgn}(x_j - x_k), \text{ and } \mathrm{sgn}(\theta) = \begin{cases} +1 & \theta > 0 \\ 0 & \theta = 0 \\ -1 & \theta < 0 \end{cases} \quad \text{(S3)}$$

where x_j and x_k are the sequential values at times j and k, respectively, and n is the length of the data set. When dealing with an asymptotically normal distribution, the mean and variance can be obtained by

$$E(S) = 0, \text{ and } Var(S) = [n(n-1)(2n+5)]/18 \quad \text{(S4)}$$

The standard normal *Z*-test statistic is computed by

$$Z = \begin{cases} \dfrac{S-1}{\sqrt{Var(S)}} & S > 0 \\ 0 & S = 0 \\ \dfrac{S+1}{\sqrt{Var(S)}} & S < 0 \end{cases} \quad \text{(S5)}$$

When $|Z| \leq Z_{1-\alpha/2}$ at the α level of significance, the null hypothesis is accepted. $Z_{1-\alpha/2}$ which is the critical value of Z from the standard normal table, the value of $Z_{1-\alpha/2}$ is 1.96 at 5% significant level. A positive Z value means an increasing trend, while a negative Z value means a decreasing trend (Douglas et al., 2000).

In the analysis of hydro-meteorological or catchment time series, the presence of autocorrelation can adversely affect the results of the Mann-Kendall (MK) test. As a remedy, the time series that exhibit significant sequential autocorrelation are subjected to trend-free pre-whitening (TFPW) procedures prior to the MK test (Yue et al., 2002; Yue et al., 2003; Aziz and Burn, 2006; Serinaldi and Kilsby, 2016; Wu et al., 2016). The TFPW method consists of three steps: (i) estimation of the trend slope to remove the trend component from the time series, (ii) estimation of $\rho 1$, which is the lag-1 autocorrelation coefficient, to eliminate or reduce the sequential autocorrelation by removing the AR(1) component from the detrended series, and (iii) reinstallation of the trend component before performing the MK test. This procedure mitigates the negative impact of autocorrelation on the accuracy of the MK test results.

S4.2 Trend-free pre-whitening Pettitt test with binary segmentation (TFPW-BS-Pettitt)

The Pettitt test is designed to detect changes in the mean values of signals against the null hypothesis of initial distribution. It utilizes the Mann-Whitney statistical function ($U_{t,T}$) to compare two independent samples ($x_1, \ldots, x_t$) and ($x_{t+1}, \ldots, x_T$), and provides the date of the change point (Pettitt, 1979; Fraedrich et al., 2001; Kam and Sheffield, 2016; Serinaldi et al., 2018). $U_{t,T}$ is computed by:

$$U_{t,T} = U_{t-1,T} + V_{t,T} \ \ (t = 2, \dots, T) \tag{S6}$$

$$V_{t,\mathrm{T}} = \sum_{j=1}^{T} \mathrm{sgn}(x_t - x_j) \tag{S7}$$

$$\mathrm{sgn}(x) = \begin{cases} -1, & x < 0 \\ 0, & x = 0 \\ +1, & x > 0 \end{cases} \tag{S8}$$

The most significant shift point is evaluated by:

$$p(t) = \max\left|U_{t,T}\right| \tag{S9}$$

The significant probability associated with a potential abrupt shift point is approximated by the following:

$$q(t) \approx 2 \cdot \exp\left(\frac{-6{U_{t,T}}^2}{T^3 + T^2}\right) \tag{S10}$$

Also, the trend-free pre-whitening (TFPW) procedure is employed in the Pettitt algorithm to mitigate the significant autocorrelation effects of non-stationary time series. However, given the Pettitt algorithm's limitation of identifying only a single abrupt shift point in a time series, it is possible for hydro-meteorological or catchment time series in non-stationary circumstances to have multiple abrupt shift points. Therefore, to detect multiple shift points, binary segmentation (BS) is used in conjunction with the Pettitt algorithm. The BS algorithm is commonly utilized in genetic testing to reduce the risk of chain failure problems during validation and improve segmentation accuracy, as demonstrated in (Lee and Verma, 2012). Specifically, the BS segments the period under Pettitt's detection through iterative processes to identify abrupt shift points in different sub-periods of the time series.

S5 Candidate driving factors

Climate forcing: Climatic factors or meteorological variables have a comprehensive response to Potential Evapotranspiration (ET_0), also referred to as reference evapotranspiration with respect to the investigation of the PRR, which in turn affects actual evapotranspiration (AET) (Liu et al., 2022; Liu et al., 2020b). ET_0 is determined by evaporative demand, which is controlled by anticyclonic conditions characterized by various atmospheric parameters such as air temperature, heat flux, wind speed, saturation vapor pressure, net radiation, and relative humidity (Hobbins et al., 2016; Liu et al., 2020a). For example, higher temperatures generally lead to increased

evapotranspiration, while high humidity limits evaporation due to abundant moisture in the air. Increased wind speeds accelerate evaporation by facilitating the departure of water molecules from the surface, thereby enhancing potential evapotranspiration. Additionally, extended sunshine hours contribute to surface energy input, fostering water evaporation and elevating potential evapotranspiration. In summary, potential evapotranspiration serves as a comprehensive indicator of the impact of climate factors on the PRR. However, from a water balance perspective, changes in external factors of precipitation-runoff links primarily related to ET_0 may not necessarily result in corresponding changes in AET. This is because AET may often be limited by moisture availability rather than energy especially in the semi-humid and semi-arid Wei River basin, thereby making the net effect of AET changes on the PRR unclear (Saft et al., 2015). Furthermore, the spatial distribution of potential evapotranspiration is closely linked to irrigation planning and management. Therefore, investigating the impact of potential evapotranspiration on PRR is of significant importance in formulating scientifically informed strategies for water resources and irrigation management (Tu et al., 2023). Given the foregoing, ET_0 is considered a climate-forcing factor in assessing the potential effects of PRR changes.

Groundwater: Groundwater, characterized by its large water storage capacity and long-term memory, plays a crucial role in the linkage between precipitation and runoff (Carlier et al., 2018). The influence of groundwater on streamflow generation varies in headwater catchments, where shallow and deep groundwater inflows contribute to streamflow with different response timescales (Hare et al., 2021). For instance, streamflow can be attributed to shallow inflow processes, such as perched saturation along hydraulic gradient fronts, exhibiting transient behavior with short response times (ranging from days to weeks) (Hirmas et al., 2018). On the other hand, discharge from unconfined aquifers exhibits slower dynamics, including trends that span multiple years. It is noteworthy that groundwater interactions extend beyond catchment boundaries, affecting groundwater quantity and regulating the exchange between regional groundwater and surface water through hydraulic gradients (Fowler et al., 2020; Bouaziz et al., 2018). Anthropogenic impacts on groundwater include sustained local groundwater extraction and modifications in vadose zone thickness (Fowler et al., 2022).

Vegetation dynamics: The effects of vegetation dynamics on the hydrological cycle refer to the influence of vegetation growth, coverage, and changes on the movement and distribution of water

within an ecosystem (Yu et al., 2023). Vegetation serves as a regulator of land-atmosphere interactions and plays a crucial role in coupling the carbon-water cycles and surface energy balance within the soil-plant-atmosphere system (Claussen et al., 2013). Vegetation interacts with the hydrological cycle through processes such as evapotranspiration, interception, infiltration, and groundwater recharge (Ajami et al., 2017). Conversely, changes in precipitation patterns, rising temperatures, and variations in water availability directly impact vegetation growth and transpiration. In recent decades, afforestation programs have been proposed to harness benefits related to flood mitigation and carbon storage. The impact of afforestation on streamflow across diverse catchments is found to consistently decrease median and low streamflow (Buechel et al., 2022). Consequently, the investigation of vegetation dynamics is underscored as a candidate driving factor in exploring the changes of PRR.

Anthropogenic influences: The intensification of anthropogenic activities, accompanied by urbanization processes such as population growth, economic development, infrastructure development, and rural-urban migration, has emerged as a global threat to the sustainability of water resources (Mekonnen and Hoekstra, 2016). However, obtaining long-term and continuous data sequences of anthropogenic activities that are linked to the hydrological cycle presents a significant challenge. Also, acquiring human activity data at the catchment level is difficult. Most associated statistical information is divided based on administrative units such as urban areas, irregular regions, or spanning multiple catchments (Thorslund and Van Vliet, 2020). Remote sensing observations offer powerful tools for analyzing and monitoring the impact of human activities on river systems globally. These observations provide extensive datasets that allow for the identification of human pressures and the assessment of their temporal progression and wide spatial distribution (Ceola et al., 2019). In addition, other anthropogenic activities related to the hydrological cycle, such as community water usage, agricultural irrigation, industrial water utilization, and the construction of reservoirs, are flexibly investigated according to the ease of data acquisition to explore their possible impacts on the PRR.

Impervious surfaces, which predominantly consist of artificial structures impeding or preventing natural water infiltration into the soil (Gong et al., 2020), constitute a key component of human settlements. They include roofs, paved surfaces, hardened grounds commonly found in human settlements, and major road surfaces (Gong et al., 2019). The Impervious Surface Ratio (ISR) is

the ratio of the impervious area to the total area of the area within a specific region. Compared with natural surfaces, impervious surfaces typically exhibit poor water permeability and possess distinct light absorption and heat capacity properties. Hence, urbanized areas characterized by high ISR values manifest a distinctive interplay between surface energy balance and water balance, influencing the occurrence and distribution of extreme precipitation and floods (Lu et al., 2019). In general, the changes in impervious surfaces affect the PRR through four primary mechanisms. (1) As the impervious surface ratio increases, the amount of surface runoff also tends to increase. Impermeable surfaces prevent water from infiltrating into the soil, resulting in a larger volume of water running off directly into streams, rivers, or stormwater drains. This can lead to increased flood risk, as well as the transport of pollutants and sediment from impervious surfaces into water bodies. (2) Increasing impervious surfaces can contribute to higher moisture retention on the surface, especially during dry months with lower potential evapotranspiration intensity. The reduced capacity of water to infiltrate the soil due to impervious surfaces leads to increased moisture retention on the surface. This can affect soil water availability, plant growth, and subsequent hydrological processes. (3) The expansion of impervious surfaces may lead to a decrease in groundwater recharge. Impermeable surfaces prevent water from percolating into the soil and impede the replenishment of groundwater stores (Shuster et al., 2005).

Night-Time Light (NTL) products provide comprehensive information regarding the influences of human presence and economic development on water resources. The luminosity of night-time light serves as an indicator for highly populated areas or regions with significant capital investments (Ceola et al., 2019). Night-time light has been widely utilized as a proxy for assessing human presence and activity across various domains, including population density, urban and rural mapping, flood risk assessment, economic analysis, and evaluation of light pollution levels (Wu et al., 2021; Ceola et al., 2019; Zhang et al., 2020). The influences of NTL on the PRR can be approached through two primary mechanisms. (1) Night-time light, through its heat emission, leads to an increase in urban temperature, thereby affecting the regional-scale hydrological cycle (Liao et al., 2017). The city acts as a warm center, increasing the unstable air mass, enhancing the convection both upwind and downwind of the urban area, and influencing the formation and distribution of precipitation (Wai et al., 2017; Zhang et al., 2020). Moreover, rising temperatures lead to increased localized evaporation, subsequently reducing surface runoff and precipitation infiltration. (2) Night-time light serves as an indicator of urbanization progress and economic

development, indirectly reflecting their impact on the PRR through anthropogenic activities (Wu et al., 2021). The intensified illumination during night-time light may signify an expansion of impervious surfaces, which affects infiltration and evaporation processes. It disrupts precipitation infiltration in certain areas, diminishes groundwater recharge from precipitation, and concentrates evaporation before and after precipitation events (Elvidge et al., 2007). Furthermore, the escalation of night-time light in conjunction with economic development also signifies increased regional water usage, resulting in reduced river flow (Vassolo and Döll, 2005). Overall, night-time light plays a dual role in the hydrological cycle. It directly influences the regional hydrological processes through alterations in the heat island effect and atmospheric stability while also indirectly reflecting the consequences of urbanization and economic development on precipitation-runoff dynamics through changes in impervious surfaces and water use.

Regions characterized by higher population densities (POP) typically exhibit increased urbanization, resulting in the proliferation of impermeable surfaces such as buildings and roads. The impacts of population density changes on the PRR can be understood through three key aspects. (1) Higher population densities lead to increased water demand for various purposes, such as domestic, industrial, and agricultural water use. The extraction of water from rivers, lakes, and groundwater sources can alter the natural flow patterns and water availability in these systems (Fang and Jawitz, 2019). (2) As population densities increase, land use may change. It implies that there is a greater need for infrastructure development, urbanization, and agricultural expansion. These activities often involve modifications to the natural landscape, including deforestation, construction of impervious surfaces (such as roads and buildings), and alteration of drainage patterns. Such land use changes can impact the hydrological cycle by affecting surface runoff, infiltration rates, and evapotranspiration processes (Hobeichi et al., 2022). (3) In regions with high population densities, the extraction of groundwater for domestic and agricultural purposes can exceed the natural replenishment rates. This overexploitation of groundwater resources can lead to groundwater depletion, reduced water availability in aquifers, and even land subsidence (Fang and Jawitz, 2019). Overall, the relationships between population density and the precipitation-runoff dynamic involve complex interactions that influence water demand, land use changes, and groundwater extraction. Understanding these factors is crucial for managing water resources sustainably in densely populated regions.

S6 Maximal Information Coefficient algorithm

The Maximal Information Coefficient (MIC), proposed by (Reshe et al., 2011), offers a measurement approach that does not rely on the distributional assumptions of datasets. This approach effectively captures extensive maximal information between variables, including both functional and non-functional relationships. When dealing with functional relationships, the MIC algorithm provides a score that is comparable to the coefficient of determination (R^2) of the datasets.

S7 Verification of DPRR based on mutual information theory

S7.1 The calculation procedure for the DPRL index

Step 1: Involve three time series: the runoff time series denoted as X_t, the precipitation time series denoted as Y_t, and an influencing factor denoted as Z_t, where $t = 1,2,\dots,n$, and n signifies the length of the time series. The initial computation entails deriving the cumulative frequency for each time series. Subsequently, the runoff time series is transformed into the following time series Q_t:

$$Q_t = \begin{cases} 1, & X_t \le X^{20} \\ 2, & X^{20} < X_t \le X^{40} \\ 3, & X^{40} < X_t \le X^{60} \\ 4, & X^{60} < X_t \le X^{80} \\ 5, & X_t > X^{80} \end{cases} \quad \text{(S11)}$$

where X^{20}, X^{40}, X^{60}, and X^{80} correspond to X_t when the cumulative frequencies are 20%, 40%, 60%, and 80%, respectively. Similar processing is applied to the precipitation time series X_t and the influencing factor Z_t, resulting in the updated time series W_t and F_t. These time series are discretized into five equidistant intervals to reduce the impact of noise while capturing a wider range of time series values across various magnitudes. Notably, the division into five equidistant boxes is a deduced outcome derived from rigorous comparative analyses and verifications (Franzen et al., 2020).

Step 2: Calculate the probability distribution functions for the time series:

$$\begin{cases} p(q_i) = \dfrac{\mathrm{count}(q_i)}{n} \\ p(w_j) = \dfrac{\mathrm{count}(w_j)}{n} \\ p(f_k) = \dfrac{\mathrm{count}(f_k)}{n} \end{cases} \tag{S12}$$

where $p(q_i)$, $p(w_j)$ and $p(f_k)$ are the probability distribution functions of Q_t, W_t and F_t respectively; $\mathrm{count}(q_i)$, $\mathrm{count}(w_j)$ and $\mathrm{count}(f_k)$ represent the occurrences of numerical values in Q_t, W_t and F_t, respectively; $i = 1,2,\ldots,5$; $j = 1,2,\ldots,5$; $k = 1,2,\ldots,5$.

Step 3: The Shannon entropy of time series is calculated as follows:

$$H(Q_t) = -\sum_{i=1}^{5} p(q_i)\log_2 p(q_i) \tag{S13}$$

where $H(Q_t)$ is the Shannon entropy of Q_t. Here, entropy with a logarithm of base 2 is considered, such that entropy and related IT measures are in units of bits.

Step 4: Calculate the joint distribution functions as follows:

$$\begin{cases} p(q_i, f_k) = \dfrac{\mathrm{count}(Q_t = q_i, F_t = f_k)}{n} \\ p(q_i, w_j) = \dfrac{\mathrm{count}(Q_t = q_i, W_t = w_j)}{n} \end{cases} \tag{S14}$$

where $p(q_i, f_k)$ is the joint distribution function of Q_t and F_t; $p(q_i, w_j)$ is the joint distribution function of Q_t and W_t; $\mathrm{count}(Q_t = q_i, F_t = f_k)$ is the number of simultaneous occurrences of $Q_t = q_i$ and $F_t = f_k$; $\mathrm{count}(Q_t = q_i, W_t = w_j)$ is the number of simultaneous occurrences of $Q_t = q_i$ and $W_t = w_j$.

Step 5: Given the influencing factor, the quantification of uncertainty within the sequence becomes feasible through the utilization of conditional entropy. This measure is computed as follows:

$$\begin{cases} H(Q_t|F_t) = \sum_{i=1}^{5}\sum_{k=1}^{5} p(q_i, f_k)\log_2 \dfrac{p(q_i, f_k)}{p(f_k)} \\ H(Q_t|W_t) = \sum_{i=1}^{5}\sum_{j=1}^{5} p(q_i, w_j)\log_2 \dfrac{p(q_i, w_j)}{p(w_j)} \end{cases} \tag{S15}$$

where $H(Q_t|F_t)$ is the conditional entropy of Q_t given F_t; $H(Q_t|W_t)$ is the conditional entropy of Q_t given W_t.

Step 6: Mutual information $I(Q_t; F_t)$, quantifies the reduction in uncertainty of one variable when another variable is known. It is the difference between entropy and conditional entropy. The calculation for mutual information is as follows:

$$I(Q_t; F_t) = H(Q_t) - H(Q_t|F_t) = \sum p(q_t, f_t)\log_2 \frac{p(q_t, f_t)}{p(q_t)p(f_t)} \quad \text{(S16)}$$

Step 7: The DPRL index is further updated as follows:

$$\mathrm{DPRL}(t) = \frac{I(Q_t; F_t)}{H(Q_t|W_t) + 1} \quad \text{(S17)}$$

where $I(Q_t; F_t)$ represents the mutual information between Q_t and F_t. It quantifies the reduction in the uncertainty of Q_t when F_t is given, providing insights into their interdependence. With regard to the impact of precipitation on runoff, this index introduces the concept of conditional entropy $H(Q_t|W_t)$, accounting for the conditional uncertainty within runoff given precipitation. Furthermore, incorporating the notion of relative error, a modification is applied to the denominator by adding +1. This adjustment prevents the denominator from becoming exceedingly small, which may lead to anomalous metric values of the index.

S7.2 Possible driving mechanisms in precipitation-runoff relationships with mutual information approach

The study applies the mutual information technique to quantitatively assess the driving levels of possible influencing factors in the precipitation-runoff relationships. The results (Figure S2b) illustrate that baseflow is the primary driving force influencing the PRR in the five sub-basins. The driving levels of baseflow are all greater than 0.4 in the five sub-basins, while the driving levels of other factors are all below 0.1. Baseflow is an important component of the Wei River Basin's runoff, particularly during the dry season (Miao et al., 2020), primarily contributing to runoff generation. Therefore, the driving levels of baseflow are higher. The impact of vegetation dynamics in WR4 and WR5 is stronger than in other sub-basins and significantly exceeds the impact of other factors in the two sub-basins. The finding aligns with the lower level of urbanization in WR4 and WR5. Furthermore, the impact of vegetation dynamics in WR5 is greater

than in WR4, illustrating that the afforestation policy in WR5 has yielded positive results (Wu et al., 2023). Additionally, compared to WR2, WR3 has a higher proportion of irrigated areas, and the typical cropping pattern in these sub-basins includes winter wheat and summer maize. The vegetation dynamics within irrigation zones depend on changes in cropping patterns, thereby exerting complex effects on the PRR within the sub-basins. The impacts of ISR, NTL, and POP in WR3 are all in the top two levels, and their impacts in WR2 are slightly smaller than those in WR3. Conversely, the impact of vegetation dynamics in WR2 is greater than that in WR3. The rapid expansion of downstream urban clusters in WR3 is a significant factor contributing to this result. Simultaneously, in pursuit of higher economic income or a more convenient lifestyle, populations in WR4 and WR5 tend to migrate towards the central cities in WR3. This migration results in lower anthropogenic driving factors for PRR in WR4 and WR5. Additionally, as populations concentrate, local surface water resources become inadequate to meet regional water demands. Consequently, groundwater extraction and inter-basin water transfer are employed to alleviate water resource pressures, leading to complex artificial interventions that may impact the PRR. ET_0 has a smaller impact on the PRR in all five sub-basins. The ranking pattern of driving levels of ET_0 in the sub-basins is similar to that of vegetation dynamics. ISR and NTL have the strongest impact in WR1, likely due to its being the smallest basin area.

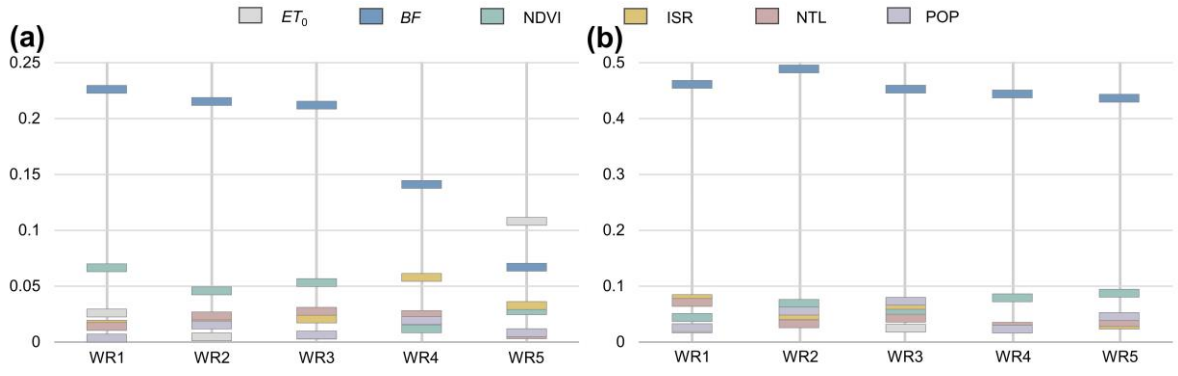

Figure S2 a, Maximum kernel density values of the absolute values of DPRR for possible influencing factors. **b,** Results of mutual information approach for possible influencing factors.

S7.3 Validation of DPRR by mutual information theory

The maximum kernel density values of the absolute values of the DPRR (Figure S2a) are employed for comparing the results of DPRR and mutual information approach. The patterns exhibited by DPRR and mutual information approach are generally consistent, which mutually validates the

reliability of their assessment outcomes. Both DPRR and mutual information approach results illustrate that baseflow is the primary factor influencing PRR. Excluding WR5, the DPRR values of baseflow are the highest among the six factors. In WR5, the DPRR value of baseflow ranks second only to ET_0. The mutual information approach values of baseflow are significantly higher than those of other factors in all five sub-basins. Furthermore, the DPRR and mutual information approach results for ISR, NTL, and POP demonstrate the differences between WR2 and WR3. WR2 is located upstream of WR3 and there is a large urban cluster downstream of WR3. Therefore, ISR, NTL, and POP have a greater impact on PRR in WR3 compared to WR2. In contrast, WR4 and WR5 have smaller urban areas, so vegetation dynamics exhibit positive impacts in DPRR results and high-level influence in mutual information approach results. However, due to the distinct foundations of DPRR and mutual information approach, which are based on nonstationary and nonlinear theories, respectively. Their results exhibit minor disparities. For instance, in WR5, the results from DPRR show that ET_0 has a much higher impact on PRR than other factors, whereas in mutual information approach results, the driving level of ET_0 is extremely low, almost equal to other factors. This disparity might be attributed to the implementation of afforestation policies in WR5, which altered the local climate, thereby causing an increase in the driving level of ET_0 on PRR during specific periods. DPRR captures the influence of ET_0 on PRR, hence demonstrating a high driving level in the maximum kernel density results.

S8 Detailed description of Figures 2, 6, and 7

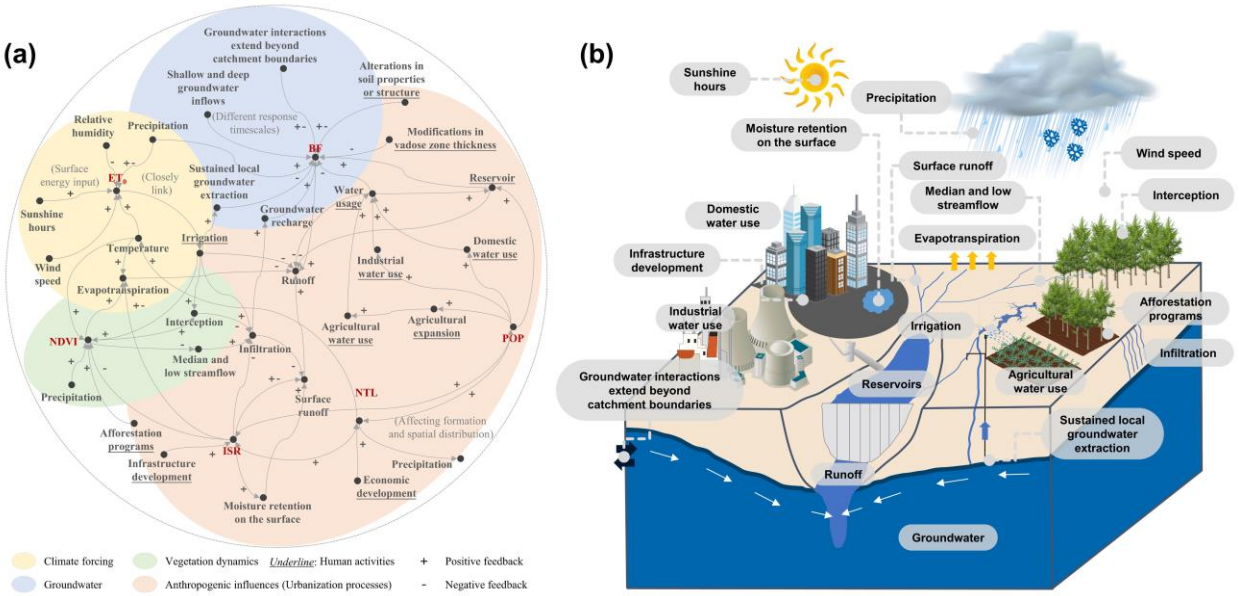

Figure S3. a, A conceptual model of catchment response developed by integrating the causal loop-based process explanations through investigating candidate driving factors. **b,** Visual synthesis of selected process explanations for potential driving mechanisms of the changes in PRR under non-stationary processes, depicting a general catchment affected by anthropogenic interference.

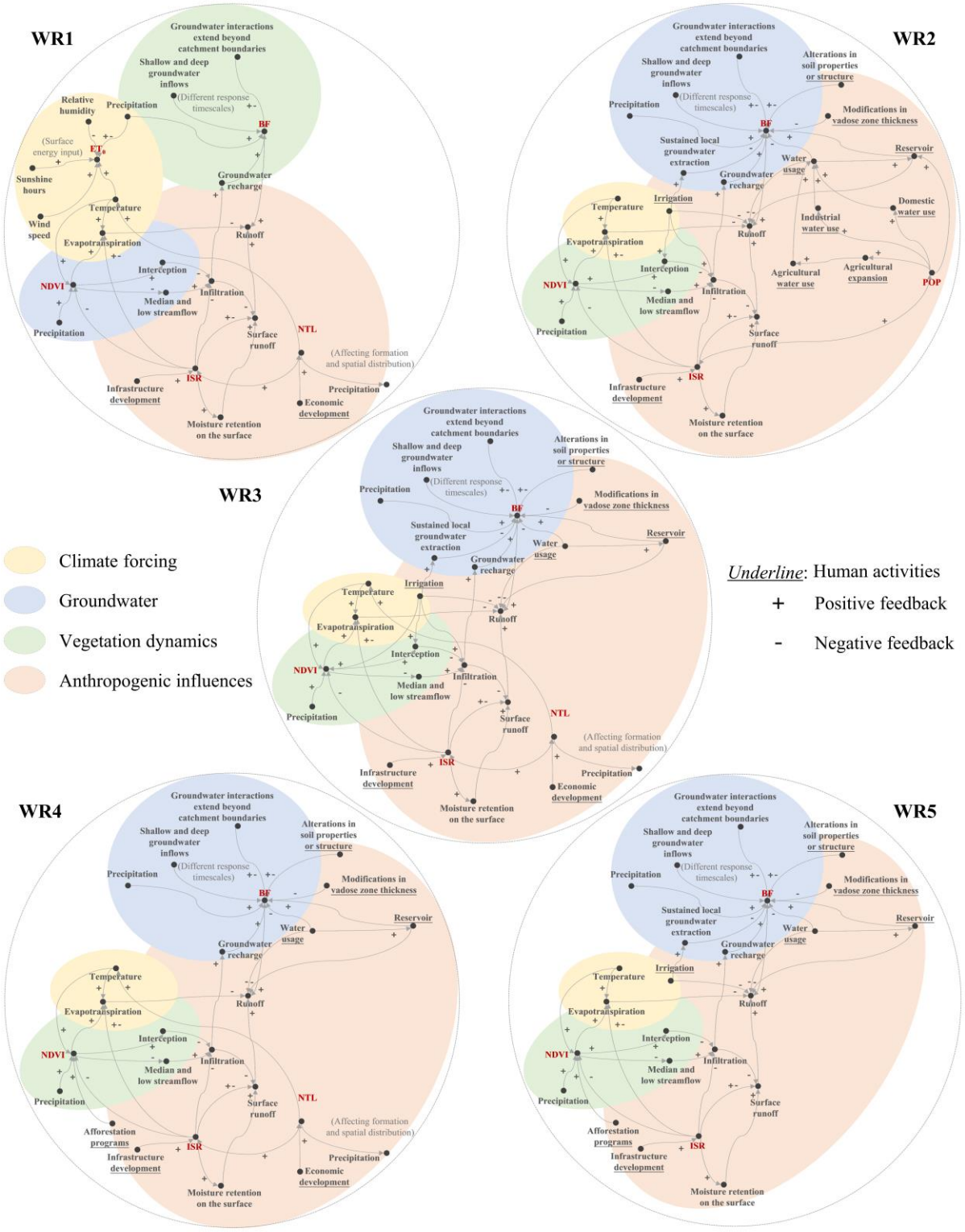

Figure S4. Causal loop diagram elucidating possible explanations of candidate driving factors in five sub-basins based on the driving levels and directions of influential factors on PRR.

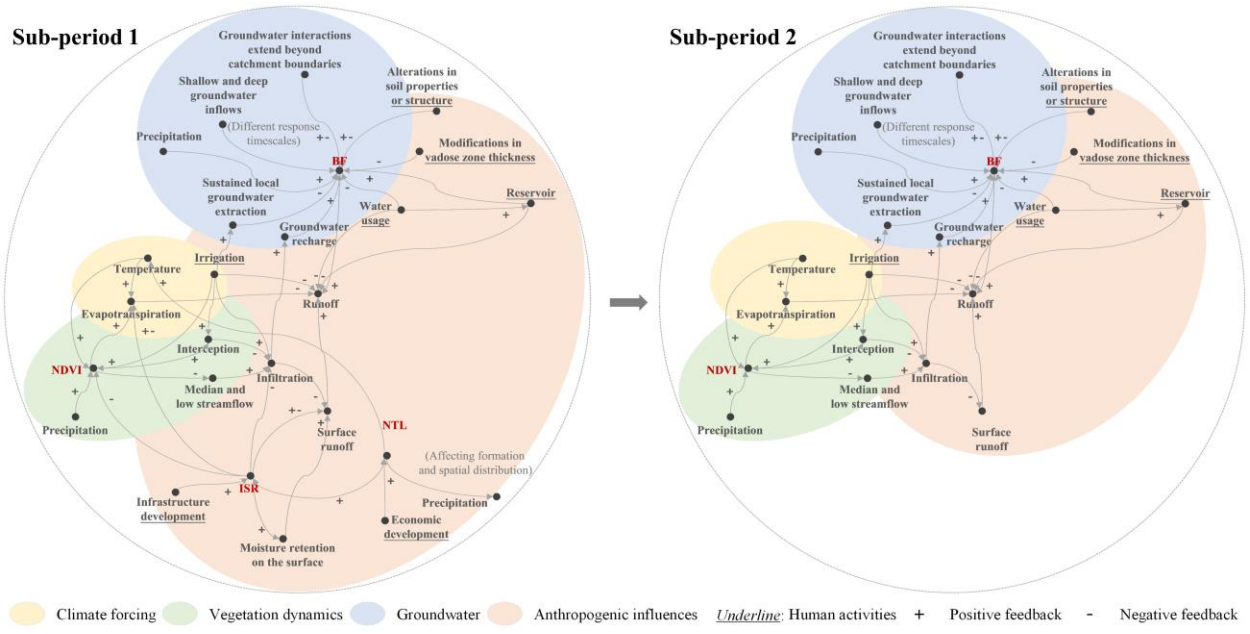

Figure S5. Causal loop diagram elucidating the potential processes controlling changes in WR3.

References

Ajami, H., Sharma, A., Band, L. E., Evans, J. P., Tuteja, N. K., Amirthanathan, G. E., and Bari, M. A.: On the non-stationarity of hydrological response in anthropogenically unaffected catchments: an Australian perspective, Hydrol. Earth Syst. Sci., 21, 281-294, https://hess.copernicus.org/articles/21/281/2017/, 2017.

Aziz, O. I. A. and Burn, D. H.: Trends and variability in the hydrological regime of the Mackenzie River Basin, J. Hydrol., 319, 282-294, https://doi.org/10.1016/j.jhydrol.2005.06.039 2006.

Bouaziz, L., Weerts, A., Schellekens, J., Sprokkereef, E., Stam, J., Savenije, H., and Hrachowitz, M.: Redressing the balance: quantifying net intercatchment groundwater flows, Hydrol. Earth Syst. Sci., 22, 6415-6434, https://hess.copernicus.org/articles/22/6415/2018/, 2018.

Buechel, M., Slater, L., and Dadson, S.: Hydrological impact of widespread afforestation in Great Britain using a large ensemble of modelled scenarios, Commun. Earth Environ., 3, 6, https://doi.org/10.1038/s43247-021-00334-0, 2022.

Cai, J., Liu, Y., Lei, T., and Pereira, L. S.: Estimating reference evapotranspiration with the FAO Penman–Monteith equation using daily weather forecast messages, Agr. Forest Meteorol., 145, 22-35, https://doi.org/10.1016/j.agrformet.2007.04.012, 2007.

Carlier, C., Wirth, S. B., Cochand, F., Hunkeler, D., and Brunner, P.: Geology controls streamflow dynamics, J. Hydrol., 566, 756-769, https://doi.org/10.1016/j.jhydrol.2018.08.069, 2018.

Ceola, S., Laio, F., and Montanari, A.: Global-scale human pressure evolution imprints on sustainability of river systems, Hydrol. Earth Syst. Sci., 23, 3933-3944, https://hess.copernicus.org/articles/23/3933/2019/, 2019.

Chapman, T.: A comparison of algorithms for stream flow recession and baseflow separation, Hydrol. Process., 13, 701-714, https://onlinelibrary.wiley.com/doi/abs/10.1002/%28SICI%291099-1085%2819990415%2913%3A5%3C701%3A%3AAID-HYP774%3E3.0.CO%3B2-2, 1999.

Claussen, M., Bathiany, S., Brovkin, V., and Kleinen, T.: Simulated climate–vegetation interaction in semi-arid regions affected by plant diversity, Nat. Geosci., 6, 954-958, https://doi.org/10.1038/ngeo1962, 2013.

Douglas, E. M., Vogel, R. M., and Kroll, C. N.: Trends in floods and low flows in the United States: impact of spatial correlation, J. Hydrol., 240, 90-105, https://doi.org/10.1016/S0022-1694(00)00336-X, 2000.

Elvidge, C. D., Tuttle, B. T., Sutton, P. C., Baugh, K. E., Howard, A. T., Milesi, C., Bhaduri, B., and Nemani, R.: Global distribution and density of constructed impervious surfaces, Sensors, 7, 1962-1979, https://www.mdpi.com/1424-8220/7/9/1962, 2007.

Fang, Y. and Jawitz, J. W.: The evolution of human population distance to water in the USA from 1790 to 2010, Nat. Commun., 10, 430, https://doi.org/10.1038/s41467-019-08366-z, 2019.

Fowler, K., Knoben, W., Peel, M., Peterson, T., Ryu, D., Saft, M., Seo, K.-W., and Western, A.: Many commonly used rainfall-runoff models lack long, slow dynamics: Implications for runoff projections, Water Resour. Res., 56, e2019WR025286, https://doi.org/10.1029/2019WR025286, 2020.

Fowler, K., Peel, M., Saft, M., Peterson, T. J., Western, A., Band, L., Petheram, C., Dharmadi, S., Tan, K. S., Zhang, L., Lane, P., Kiem, A., Marshall, L., Griebel, A., Medlyn, B. E., Ryu, D., Bonotto, G., Wasko, C., Ukkola, A., Stephens, C., Frost, A., Gardiya Weligamage, H., Saco, P., Zheng, H., Chiew, F., Daly, E., Walker, G., Vervoort, R. W., Hughes, J., Trotter, L., Neal, B., Cartwright, I., and Nathan, R.: Explaining changes in rainfall–runoff relationships during and after Australia's Millennium Drought: a community perspective, Hydrol. Earth Syst. Sci., 26, 6073-6120, https://hess.copernicus.org/articles/26/6073/2022/, 2022.

Fraedrich, K., Gerstengarbe, F. W., and Werner, P. C.: Climate shifts during the last century, Clim. Change, 50, 405-417, https://doi.org/10.1023/a:1010699428863, 2001.

Franzen, S. E., Farahani, M. A., and Goodwell, A. E.: Information Flows: Characterizing precipitation-streamflow dependencies in the Colorado headwaters with an information theory approach, Water Resour. Res., 56, e2019WR026133, https://doi.org/10.1029/2019WR026133, 2020.

Gong, P., Li, X., and Zhang, W.: 40-Year (1978–2017) human settlement changes in China reflected by impervious surfaces from satellite remote sensing, Sci. Bull., 64, 756-763, https://doi.org/10.1016/j.scib.2019.04.024, 2019.

Gong, P., Li, X., Wang, J., Bai, Y., Chen, B., Hu, T., Liu, X., Xu, B., Yang, J., Zhang, W., and Zhou, Y.: Annual maps of global artificial impervious area (GAIA) between 1985 and 2018, Remote Sens. Environ., 236, 111510, https://doi.org/10.1016/j.rse.2019.111510, 2020.

Hare, D. K., Helton, A. M., Johnson, Z. C., Lane, J. W., and Briggs, M. A.: Continental-scale analysis of shallow and deep groundwater contributions to streams, Nat. Commun., 12, 1450, https://doi.org/10.1038/s41467-021-21651-0, 2021.

Hirmas, D. R., Giménez, D., Nemes, A., Kerry, R., Brunsell, N. A., and Wilson, C. J.: Climate-induced changes in continental-scale soil macroporosity may intensify water cycle, Nature, 561, 100-103, https://doi.org/10.1038/s41586-018-0463-x, 2018.

Hobbins, M., Senay, G., Gowda, P. H., and Artan, G.: Evapotranspiration and evaporative demand, Statistical Analysis of Hydrologic Variables: Methods and Applications, 71-143, https://doi.org/10.1061/9780784415177.ch03, 2016.

Hobeichi, S., Abramowitz, G., Ukkola, A. M., De Kauwe, M., Pitman, A., Evans, J. P., and Beck, H.: Reconciling historical changes in the hydrological cycle over land, Npj Clim. Atmos. Sci., 5, 17, https://doi.org/10.1038/s41612-022-00240-y, 2022.

Hu, C., Zhao, D., and Jian, S.: Baseflow estimation in typical catchments in the Yellow River Basin, China, Water Supply, 21, 648-667, https://doi.org/10.2166/ws.2020.338, 2021.

Kam, J. H. and Sheffield, J.: Changes in the low flow regime over the eastern United States (1962–2011): variability, trends, and attributions, Clim. Change, 135, 639-653, https://doi.org/10.1007/s10584-015-1574-0, 2016.

Lee, H. and Verma, B.: Binary segmentation algorithm for English cursive handwriting recognition, Pattern Recogn., 45, 1306-1317, https://doi.org/10.1016/j.patcog.2011.09.015, 2012.

Liao, W., Liu, X., Wang, D., and Sheng, Y.: The impact of energy consumption on the surface urban heat island in China's 32 major cities, Remote Sens., 9, 250, https://www.mdpi.com/2072-4292/9/3/250, 2017.

Liu, Y., Yu, L., and Chen, G.: Characterization of sea surface temperature and air-sea heat flux anomalies associated with mesoscale eddies in the South China Sea, Journal of Geophysical Research: Oceans, 125, e2019JC015470, https://doi.org/10.1029/2019JC015470, 2020a.

Liu, Y., Jiang, Q., Wang, Q., Jin, Y., Yue, Q., Yu, J., Zheng, Y., Jiang, W., and Yao, X.: The divergence between potential and actual evapotranspiration: An insight from climate, water, and vegetation change, Sci. Total Environ., 807, 150648, https://doi.org/10.1016/j.scitotenv.2021.150648, 2022.

Liu, Z., Cheng, L., Zhou, G., Chen, X., Lin, K., Zhang, W., Chen, X., and Zhou, P.: Global response of evapotranspiration ratio to climate conditions and watershed characteristics in a changing environment, J. Geophys. Res-Atmos., 125, e2020JD032371, https://doi.org/10.1029/2020JD032371, 2020b.

Lu, M., Xu, Y., Shan, N., Wang, Q., Yuan, J., and Wang, J.: Effect of urbanisation on extreme precipitation based on nonstationary models in the Yangtze River Delta metropolitan region, Sci. Total Environ., 673, 64-73, https://doi.org/10.1016/j.scitotenv.2019.03.413, 2019.

Mekonnen, M. M. and Hoekstra, A. Y.: Four billion people facing severe water scarcity, Sci. Adv., 2, e1500323, https://www.science.org/doi/abs/10.1126/sciadv.1500323, 2016.

Miao, C., Zheng, H., Jiao, J., Feng, X., Duan, Q., and Mpofu, E.: The changing relationship between rainfall and surface runoff on the Loess Plateau, China, J. Geophys. Res-Atmos., 125, e2019JD032053, https://doi.org/10.1029/2019JD032053, 2020.

Pettitt, A. N.: A non-parametric approach to the change-point problem, Appl. Stat., 28, 126-135, https://doi.org/10.2307/2346729 1979.

Reshe, D. N., Reshef, Y. A., Finucane, H. K., Grossman, S. R., McVean, G., Turnbaugh, P. J., Lander, E. S., Mitzenmacher, M., and Sabeti, P. C.: Detecting novel associations in large data sets, Science, 334, 1518-1524, https://doi.org/10.1126/science.1205438, 2011.

Saft, M., Western, A. W., Zhang, L., Peel, M. C., and Potter, N. J.: The influence of multiyear drought on the annual rainfall-runoff relationship: An Australian perspective, Water Resour. Res., 51, 2444-2463, https://doi.org/10.1002/2014WR015348, 2015.

Serinaldi, F. and Kilsby, C. G.: The importance of prewhitening in change point analysis under persistence, Stoch. Environ. Res. Risk Assess., 30, 763-777, https://doi.org/10.1007/s00477-015-1041-5, 2016.

Serinaldi, F., Kilsby, C. G., and Lombardo, F.: Untenable nonstationarity: An assessment of the fitness for purpose of trend tests in hydrology, Adv. Water Resour., 111, 132-155, https://doi.org/10.1016/j.advwatres.2017.10.015, 2018.

Shuster, W. D., Bonta, J., Thurston, H., Warnemuende, E., and Smith, D.: Impacts of impervious surface on watershed hydrology: A review, Urban Water J., 2, 263-275, https://doi.org/10.1080/15730620500386529, 2005.

Thorslund, J. and van Vliet, M. T. H.: A global dataset of surface water and groundwater salinity measurements from 1980–2019, Sci. Data, 7, 231, https://doi.org/10.1038/s41597-020-0562-z, 2020.

Tu, Z., Yang, Y., Roderick, M. L., and McVicar, T. R.: Potential evaporation and the complementary relationship, Water Resour. Res., 59, e2022WR033763, https://doi.org/10.1029/2022WR033763, 2023.

Vassolo, S. and Döll, P.: Global-scale gridded estimates of thermoelectric power and manufacturing water use, Water Resour. Res., 41, https://doi.org/10.1029/2004WR003360, 2005.

Wai, K. M., Wang, X. M., Lin, T. H., Wong, M. S., Zeng, S. K., He, N., Ng, E., Lau, K., and Wang, D. H.: Observational evidence of a long-term increase in precipitation due to urbanization effects and its implications for sustainable urban living, Sci. Total Environ., 599-600, 647-654, https://doi.org/10.1016/j.scitotenv.2017.05.014, 2017.

Wu, C., Xie, J., Qiu, D., Xie, Z., Gao, P., and Mu, X.: Effects of climate change and anthropogenic activities on runoff change of the Weihe River basin, Northwest China, River Res. Appl., 39, 648-660, https://doi.org/10.1002/rra.4102, 2023.

Wu, J., Chen, Y., and Hang, Q.: Analysis of Inconsistent Hydrological Frequency Based on TFPW-MK-Pettitt and EEMD, Environmental Science and Sustainable Development: International Conference on Environmental Science and Sustainable Development (ICESSD 2015), 198-207,

Wu, W.-B., Ma, J., Meadows, M. E., Banzhaf, E., Huang, T.-Y., Liu, Y.-F., and Zhao, B.: Spatio-temporal changes in urban green space in 107 Chinese cities (1990–2019): The role of economic drivers and policy, Int. J. Appl. Earth Obs., 103, 102525, https://doi.org/10.1016/j.jag.2021.102525, 2021.

Yu, S., Qin, H., and Ding, W.: Modeling the effects of vegetation dynamics on the hydrological performance of a bioretention system, J. Hydrol., 620, 129473, https://doi.org/10.1016/j.jhydrol.2023.129473, 2023.

Yue, S., Pilon, P., and Phinney, B.: Canadian streamflow trend detection: impacts of serial and cross-correlation, Hydrolog. Sci. J., 48, 51-63, https://doi.org/10.1623/hysj.48.1.51.43478 2003.

Yue, S., Pilon, P., Phinney, B., and Cavadias, G.: The influence of autocorrelation on the ability to detect trend in hydrological series, Hydrol. Process., 16, 1807-1829, https://doi.org/10.1002/hyp.1095 2002.

Zhang, L., Chen, X., and Lai, R.: Urban signatures of sub-daily extreme precipitation events over a metropolitan region, Atmos. Res., 246, 105204, https://doi.org/10.1016/j.atmosres.2020.105204, 2020.